analytical chemistry

Article

pubs.acs.org/ac

Viscoelastic Separation of Particles by Size in Straight Rectangular Microchannels: A Parametric Study for a Refined Understanding

Di Li, Xinyu Lu, and Xiangchun Xuan*

Department of Mechanical Engineering, Clemson University, Clemson, South Carolina 29634-0921, United States

Supporting Information

ABSTRACT: Microfluidic separation of particles has been implemented using a variety of force fields. We demonstrate in this work a continuous sheath-free separation of both a binary and a ternary particle mixture in viscoelastic polymer solutions through straight rectangular microchannels. This label-free separation arises from the flow-induced lift force that directs particles toward size-sensitive focusing positions in a high width/height channel. It is found to be a strong function of multiple experimental parameters, which is systematically investigated in terms of dimensionless numbers. We propose to explain the observed lateral shifting of particle focusing positions as a result of the competing center- (due to fluid elasticity effects) and wall- (due to fluid elasticity and shear thinning effects) directed elastic lift forces. The inertial lift force comes into effect at relatively high flow rates, which appears to reduce the separation efficiency and purity in our experiments.

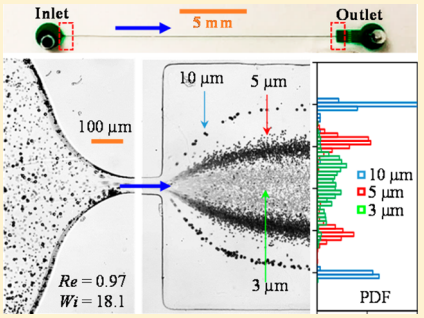

Separating targeted particles (either biological or synthetic) from a mixture in a continuous flow is important to many biological, chemical, and environmental applications. It has been implemented in microfluidic devices[1−5] by the use of a variety of force fields including acoustic,[6,7] electric,[8,9] hydrodynamic,[10,11] magnetic,[12,13] and optical,[14,15] etc. Among these forces, the flow-induced inertial lift in Newtonian fluids[16,17] has recently been extensively studied for high-throughput particle separations.[18,19] More recently, the hydrodynamic lift induced in non-Newtonian fluid flows has been demonstrated with the capability of manipulating particles with a much smaller size[20,21] and at a much higher throughput[22] than in Newtonian fluids. This elasto-inertial lift[23−25] has been exploited by several research groups to achieve the focusing of various types of particles in viscoelastic fluids through straight cylindrical[26−28] or rectangular[29−32] microchannels. It has also been combined with the Dean flow to realize the single-line particle focusing in curved microchannels.[33−36] Such two- or three-dimensional focusing effects have been utilized to align particles for enhanced detection and analysis.[37−39]

Continuous-flow particle separation in viscoelastic fluids has been implemented in conjunction with a sheath flow focusing, where the particle-free sheath fluid can be either Newtonian or non-Newtonian. In the former case, larger particles migrate across the interface of the non-Newtonian particle solution and the Newtonian sheath fluid, leaving smaller particles restrained in the non-Newtonian solution[40] due to the particle-size dependent elastic lift.[41] For the case with a non-Newtonian sheath fluid, particles have been observed to migrate toward both size[42−46] and shape[47] dependent lateral positions. Sheath-free particle separation has also been demonstrated in viscoelastic fluid flows. In a bifurcating microchannel, particles are elasto-inertially focused to the center of the main-branch (either cylindrical[48,49] or slit-like[50]) and then displaced away from the sidewall of each rectangular side-branch at a particle-size dependent rate. In a simple straight square microchannel, large particles can be selectively enriched and filtered from a binary particle mixture[51] due to the single-line elasto-inertial particle focusing effect.[52] In a similar-shaped microchannel, fresh red blood cells are found to be directed toward the centerline by the deformability-induced lift while more rigid white blood cells and fixed red blood cells are both entrained at the corners by the elastic lift under a negligible fluid inertia.[53]

Very recently particles have been observed to migrate toward both size[54] and shape[55] dependent equilibrium positions in viscoelastic fluid flows through straight rectangular microchannels with a high width/height ratio. Each of these differential focusing phenomena can yield a continuous particle separation with a high efficiency and purity. However, a comprehensive understanding of the important factors, especially the fluid properties, that affect the size-based particle separation in viscoelastic fluids is still lacking. We present in this work a systematic experimental study of multiple parametric effects on a binary particle separation for a refined understanding of the underlying particle migration and focusing mechanism. Moreover, we demonstrate a sheathless viscoelastic separation of a ternary mixture of particles with close sizes, which can potentially be further extended to a heterogeneous particle mixture.

EXPERIMENTAL SECTION

Three sizes of spherical polystyrene particles with diameters of 3, 5, and 10 μm (Sigma-Aldrich) were used for separations.

Received: September 5, 2016
Accepted: November 18, 2016
Published: November 18, 2016

ACS Publications © 2016 American Chemical Society

DOI: 10.1021/acs.analchem.6b03501
Anal. Chem. 2016, 88, 12303−12309

They were resuspended in water or aqueous polymer solutions to a final concentration of 10^6–10^7 particles per milliliter each. Three types of polymers, poly(ethylene oxide) (PEO, molecular weight M_w = 2 × 10^6 Da, Sigma-Aldrich), Polyvinylpyrrolidone (PVP, M_w = 0.36 × 10^6 Da, Sigma-Aldrich), and polyacrylamide (PAA, M_w = 18 × 10^6 Da, Polysciences), were used to prepare the viscoelastic fluids. PEO solutions were made at 500, 1000, and 2000 ppm. The 1000 ppm PEO solution was also mixed with glycerol at two different weight percentages, 15% and 45%, to vary the solvent viscosity. The PVP solution was made at 8% (weight percentage), and the PAA solution was at 50 ppm, both of which are often used for particle manipulations.[26−31,38,48,51] The rheology properties of these polymer solutions (see the Supporting Information on how they were obtained) are summarized in Table 1.

Table 1. Rheology Properties of the Prepared Polymer Solutions at 20 °C

	PEO concentration (c, ppm)			PEO/glycerol (wt %)		PVP (wt %)	PAA (ppm)
properties	500	1000	2000	15	45	8	50
density ρ (g/cm^3)	1.0	1.0	1.0	1.03	1.10	1.05	1.0
zero-shear viscosity η_0 (mPa s)	1.8	2.3	4.1	2.96	9.03	140	1.8
effective relaxation time λ_e (ms)	4.3	6.8	10.6	11.0	24.0	2.3	10

Microchannels were fabricated with polydimethylsiloxane (PDMS) using the standard soft lithography technique as described elsewhere.[56] They are each 20 mm long and 50 μm wide with three different heights: 15, 25, and 40 μm. The outlet of each microchannel is connected with a 2 mm long, 900 μm wide expansion for enhanced particle separation and visualization. A top view picture of the microchannel is shown in Figure 1A. Particulate flows were driven by a syringe pump

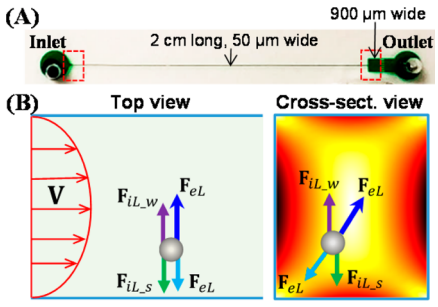

Figure 1. (A) Top-view picture of the straight rectangular microchannel used in experiments, where the two dashed-line boxes highlight the windows of view at the inlet and the outlet expansion, respectively. (B) Force analysis on a particle in a viscoelastic fluid flow through a straight rectangular microchannel: the fluid elasticity-induced lift, F_{eL}, directs the particle toward the channel center and four corners where the fluid shear rate is the lowest;[20,43,51,53,54] the wall-induced inertial lift, F_{iL_w}, and the shear gradient-induced inertial lift, F_{iL_s}, direct the particle toward the channel center and wall, respectively.[16−19] The parabolic profile of fluid velocity, V, is illustrated in the top view of the microchannel (left panel). The contour of fluid shear rate is indicated by the color in the cross-sectional view (right panel, the darker the larger).

(KD Scientific), where particle motion was visualized through an inverted microscope (Nikon Eclipse TE2000U, Nikon Instruments) with a CCD camera (Nikon DS-Qi1Mc). Superimposed images were produced by stacking sequential images using the Nikon imaging software (NIS-Elements). The particle center positions at the outlet expansion were analyzed using ImageJ software (National Institute of Health) and plotted as the probability distribution function (PDF) in Excel (Microsoft).

THEORETICAL SECTION

Mechanism of Particle Separation. As shown schematically in Figure 1B, a particle experiences both elastic and inertial lift forces in a viscoelastic fluid flow through a straight rectangular microchannel. The elastic lift, F_{eL}, is generated by the nonuniform normal stress differences,[57−59] where the first normal stress difference, N_1, creates an extra tension along the streamlines and the second normal stress difference,[60] N_2, produces a secondary flow over the channel cross-section.[61] Considering the magnitude of N_2 is usually much smaller than that of N_1,[60] we assume F_{eL} is proportional to the variation of N_1 over the size of the particle,[29,55]

$$F_{eL} \sim a^3 \nabla N_1 \sim \lambda_e (a/w)^3 Q^3 \quad (1)$$

where a is the (equivalent) spherical diameter of the particle, λ_e is the effective relaxation time of the fluid (see Table 1), w is the channel width, and Q is the volumetric flow rate. This transverse elastic force directs the particle toward the low shear rate (see the contour in the right panel of Figure 1B, where the darker color indicates a larger shear rate) regions, i.e., the centerline and corners of the microchannel.[20,43,51,53,54]

The inertial lift force is often broken down into two parts for a neutrally buoyant particle:[16−19] the wall-induced lift, F_{iL_w}, is a result of the pressure increase between a particle and its adjacent channel wall, which pushes the particle away from the wall; the shear gradient-induced inertial lift, F_{iL_s}, is a result of the curvature of the velocity profile in Poiseuille flow, which directs the particle toward the high shear rate regions, i.e., the channel walls. The total inertial lift, F_{iL}, exerted on a particle is given by[17−19,55]

$$F_{iL} = F_{iL\_w} + F_{iL\_s} \sim \rho V^2 a^4 / w^2 \sim \rho (a/w)^4 Q^2 \quad (2)$$

where ρ is the fluid density, and V is the average fluid velocity. As the elastic lift, F_{eL} and the inertial lift, F_{iL}, scale differently with the (equivalent) spherical diameter, particles with dissimilar sizes are focused to distinct equilibrium positions enabling a continuous sheath-free high-efficiency separation.[54,55] Moreover, the relaxation time, fluid flow rate, and channel dimensions can each be varied to change F_{iL} and/or F_{eL} and hence tune the equilibrium particle positions for an enhanced viscoelastic separation.

Dimensionless Numbers. Four dimensionless numbers are defined to characterize the fluid and particle dynamics in viscoelastic flows through straight rectangular microchannels. The (channel) Reynolds number, Re, compares the inertial force to viscous force,

$$Re = \frac{\rho V D_h}{\eta_0} = \frac{2\rho Q}{\eta_0 (w + h)} \quad (3)$$

where $D_h = 2wh/(w + h)$ is the hydraulic diameter for a rectangular microchannel of width w and height h, and η_0 is the

DOI: 10.1021/acs.analchem.6b03501
Anal. Chem. 2016, 88, 12303−12309

zero-shear fluid viscosity. The Weissenberg number, *Wi*, compares the elastic force to viscous force,

$$Wi = \lambda_e \dot{\gamma} = \lambda_e \frac{2V}{w} = \frac{2\lambda_e Q}{w^2 h} \quad (4)$$

where $\dot{\gamma}$ is the average fluid shear rate in the width direction of the microchannel. The elasticity number, *El*, is the ratio of the Weissenberg number to Reynolds umber,

$$El = \frac{Wi}{Re} = \frac{\lambda_e \eta_0 (w + h)}{\rho w^2 h} \quad (5)$$

which compares the elastic force to inertial force and is independent of the flow kinematics. The channel aspect ratio, AR, is defined as the ratio of the channel width to height,

$$AR = w/h \quad (6)$$

RESULTS AND DISCUSSION

Binary Particle Separation. Figure 2 demonstrates the viscoelastic separation of 5 μm- and 10 μm-diameter spherical particles in 1000 ppm PEO solution through a straight rectangular microchannel. The channel is 50 μm wide and 25 μm high with an aspect ratio of AR = 2.0. The volume flow rate is 250 μL/h, at which *Re* = 0.81 and *Wi* = 15.1. The snapshot image at the channel inlet (Figure 2, top) shows a uniform distribution of the binary particle mixture. The superimposed image at the outlet expansion (Figure 2, bottom) indicates the formation of four distinct tight particle streams that are symmetric with respect to the channel centerline. The two outer streams are 10 μm particles and each about 1/3 of the channel half-width away from the sidewalls. The two inner streams are 5 μm particles and each off the channel center by 1/3 of the channel half-width. This observation that the focusing positions of larger particles are further away from the channel center is consistent with a recent study,[54] which might be related to the additional "equilibrium" particle positions (other than the channel centerline and corners[20,43,51,53,54]) in a shear-thinning fluid that arises from the secondary flow within the channel cross-section as a result of the second normal stress difference.[62] It is important to note that each observed particle equilibrium position in Figure 2 may actually represent two focused particle streams at different focal planes, which has been verified to occur in inertial particle focusing via the confocal imaging.[63] This direction deserves further studies.

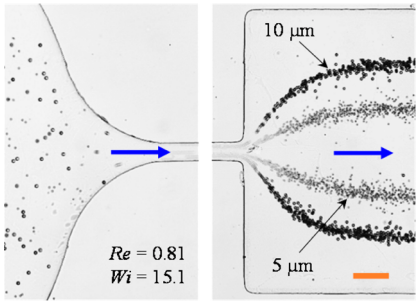

Figure 2. Continuous separation of 5 μm- and 10 μm-diameter spherical particles in 1000 ppm PEO solution through a straight 50 μm-wide and 25 μm-high rectangular microchannel at a flow rate of 250 μL/h: (left) snapshot image at the channel inlet and (right) superimposed image at the outlet expansion. The block arrows indicate the flow direction. The scale bar represents 100 μm.

Previous studies have indicated that the inertial lift, F_{iL}, focuses particles in Newtonian fluids toward the center-plane of a microchannel with AR = 2.0 if the particle Reynolds number, $Re_p = Re(a/D_h)^2$, grows to the order of 1.[16−19] However, as *Re* = 0.81 in the current experiment, at which $Re_p = 0.07 < 0.1$ for even 10 μm particles, it should be primarily the elastic lift, F_{eL}, that creates the off-center particle focusing in Figure 2. To explain the observed particle separation in Figure 2, we propose that analogous to F_{iL},[16−19] F_{eL} can also be broken down into two components where one points toward the channel center, $F_{eL\to c}$, due to fluid elastic effects.[20,43,51,53,54,57−59] The other component is toward the wall, $F_{eL\to w}$, due to fluid elasticity[20,43,44,51,53,57−59] and shear-thinning[28,59,64] effects, which are effective at relatively low and high flow rates, respectively. Moreover, $F_{eL\to w}$ is a stronger function of particle size than $F_{eL\to c}$, which drives the off-center shift of the viscoelastic focusing positions of larger particles. The effects of flow rate, fluid elasticity, and channel geometry on these proposed elastic lift components and in turn the viscoelastic particle focusing and separation are presented in the following subsections. We note that particles are able to reach their equilibrium positions under our experimental conditions, which is verified using the dimensionless "focusing" number defined by Romeo et al.[65] (see a quantitative analysis in the Supporting Information).

Effects of Flow Rate in Terms of Re and Wi. Figure 3 shows the flow rate effect on the separation of 5 and 10 μm particles in 1000 ppm PEO solution through a 25 μm-deep microchannel. The increase of flow rate, *Q*, raises the values of both *Re* and *Wi* (labeled on the cropped superimposed images in Figure 3), leading to larger F_{iL} and F_{eL}. At *Q* = 50 μL/h where F_{iL} is negligible at *Re* = 0.16, the majority of 5 μm particles are focused into a single band around the center of the microchannel (better viewed from the PDF plot in Figure 3) due to the dominant impact of $F_{eL\to c}$ over $F_{eL\to w}$. In contrast, all 10 μm particles are focused into two tight streams that are each halfway of the channel half-width due to the stronger

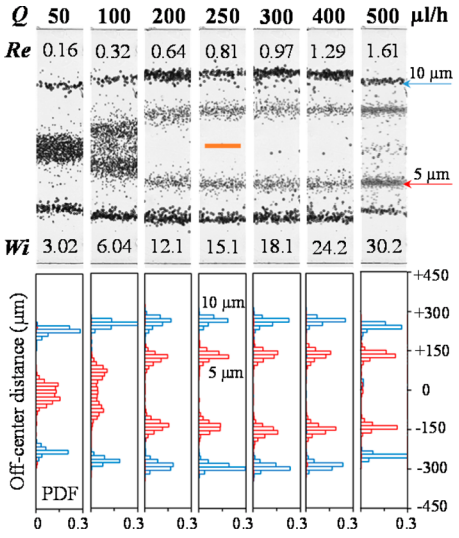

Figure 3. Effects of flow rate (in terms of *Re* and *Wi* with values being labeled) on the separation of 5 and 10 μm particles in 1000 ppm PEO solution through a straight 50 μm-wide and 25 μm-high rectangular microchannel: (top) superimposed images (cropped) and (bottom) particle PDF plots at the outlet expansion. The scale bar represents 100 μm.

DOI: 10.1021/acs.analchem.6b03501
Anal. Chem. 2016, 88, 12303−12309

dependence of $F_{eL\rightarrow w}$ on particle size than $F_{eL\rightarrow c}$ as noted above. With the increase of flow rate until Q = 250 μL/h, the single band of 5 μm particles is gradually split into two off-center streams that each shifts toward 1/3 of the channel half-width. Meanwhile, the two streams of 10 μm particles still stay tight and each slowly shifts outward until 2/3 of the channel half-width. This trend, as viewed from both the particle images and PDF plots in Figure 3, may be explained by the greater scaling of $F_{eL\rightarrow w}$ with flow rate as compared to $F_{eL\rightarrow c}$.

At Q = 300 μL/h with Re = 0.97, the focusing positions of both types of particles remain nearly identical to those at Q = 250 μL/h though a very small number of 10 μm particles start appearing at the channel center. This phenomenon may probably be a result of the action of F_{iL}, which pushes particles toward the channel center. Consequently, with increasing flow rates all the focused particle streams slowly shift inward. Moreover, 5 μm particles also reappear in the channel center along with 10 μm particles due to the effect of F_{iL}. This transition from single to dual to triple equilibrium positions in viscoelastic particle focusing is consistent with the observation in previous studies.[54,55] It is a result of the competition between the two components of elastic lift, $F_{eL\rightarrow c}$ and $F_{eL\rightarrow w}$, at Q < 300 μL/h with Re < 1, and the competition between the elastic and inertial lifts, F_{eL} and F_{iL}, at higher flow rates with $Re \geq 1$. The best separation is achieved at around Q = 250 μL/h, which lies at the border of these two regimes.

Effects of PEO Concentration in Terms of El. Figure 4 shows the PEO concentration effect on the viscoelastic separation of 5 and 10 μm particles in a 25 μm-deep microchannel under three different flow rates: Q = 50, 250, and 500 μL/h. Both particle images (see images at other flow rates in Figure S-1 of the Supporting Information) and 3D plots for particle PDF at the channel outlet are displayed. In water (i.e., 0 ppm PEO solution) without elasticity, no separation is observed because, as noted above, the two types of particles are both (weakly) focused by F_{iL} toward the channel centerline.[16−19,66] Increasing the concentration of PEO raises Wi and reduces Re due to the increased relaxation time and fluid viscosity (see Table 1), leading to a greater El or equivalently an enhanced contribution of F_{eL} (see the calculated values of Re, Wi, and El for all the polymer solutions used in our experiments in Table S-1 of the Supporting Information). In 500 ppm PEO solution, the viscoelastic focusing is apparently weaker than in 1000 ppm for both 5 and 10 μm particles. Interestingly, 10 μm particles seem to have four equilibrium positions at Q = 50 μL/h, where two are still halfway to the channel centerline while the other two are each about 1/6 of the channel half-width away from the sidewall. The mechanism behind this observation is currently unclear. In addition, 10 μm particles start being focused toward the channel center at a lower flow rate than in 1000 ppm PEO. This phenomenon is attributed to the weakened contribution of F_{eL} in 500 ppm PEO with a smaller El whereas the influence of F_{iL} grows due to the greater Re than in 1000 ppm PEO. The enhanced fluid elasticity in 2000 ppm PEO solution further shifts the particle focusing positions inward due to the larger role of $F_{eL\rightarrow c}$ than $F_{eL\rightarrow w}$. However, the occurrence of 10 μm particles along the channel center in 2000 ppm PEO is delayed as compared to 1000 ppm PEO solution. This may be due to the reduced role of F_{iL} in 2000 ppm PEO with a smaller Re and a larger El, which is opposite to that in 500 ppm as explained above.

Effects of Solvent Viscosity in Terms of El. Figure 5 shows the solvent viscosity effect on the viscoelastic separation of 5 and 10 μm particles in 1000 ppm PEO solution through a 25 μm-deep microchannel under different flow rates. Adding glycerol into the PEO solution increases its viscosity as well as relaxation time, which causes similar variations in Re and Wi to those at a higher PEO concentration. A similar shifting of particle focusing positions toward the channel centerline is thus expected, which is illustrated in Figure 5 when the glycerol content is increased from 15 to 45 wt %. However, this inward shifting is not obvious when 15 wt % glycerol is added to the pure PEO solution (refer to the images in Figure 3). In addition, the particle focusing positions in each of these PEO/glycerol solutions undergo a similar trend to those in the pure PEO solution when the flow rate is increased, i.e., first move outward due to the stronger action of $F_{eL\rightarrow w}$ than $F_{eL\rightarrow c}$ at low flow rates and then move inward due to probably the increased contribution of F_{iL} as explained earlier.

Effects of Polymer Type in Terms of El. Figure 6 compares the separations of 5 and 10 μm particles in three commonly

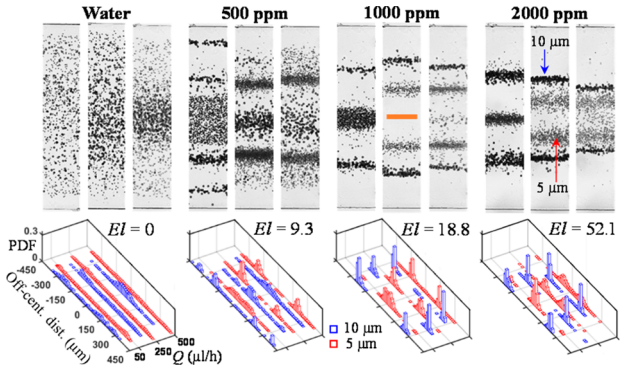

Figure 4. Effects of PEO concentration (in terms of El with values being labeled) on the viscoelastic separation of 5 and 10 μm particles through a straight 50 μm-wide and 25 μm-high rectangular microchannel: (top) superimposed images (cropped) at flow rates of 50, 250, and 500 μL/h from left to right and (bottom) 3D plots of particle PDF at the outlet expansion. The scale bar represents 100 μm.

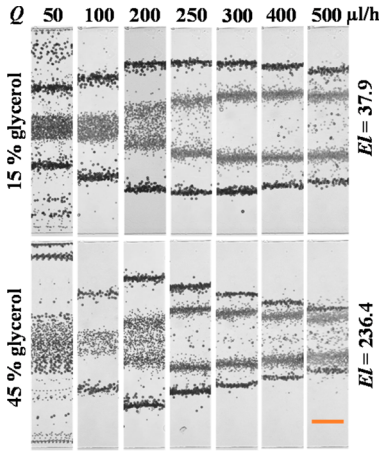

Figure 5. Effects of solvent viscosity (in terms of El with values being labeled), which is varied by adding glycerol (wt %) into 1000 ppm PEO solution, on the viscoelastic separation of 5 and 10 μm particles through a straight 50 μm-wide and 25 μm-high rectangular microchannel under a range of flow rates. The scale bar represents 100 μm.

DOI: 10.1021/acs.analchem.6b03501
Anal. Chem. 2016, 88, 12303−12309

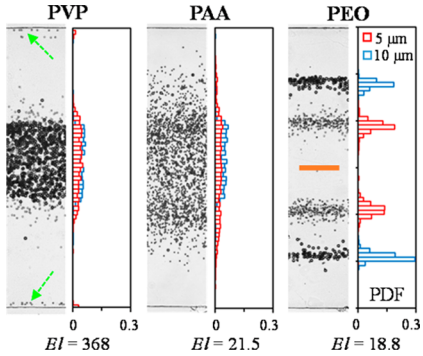

Figure 6. Comparison of the binary separations of 5 and 10 μm particles in three commonly used polymer solutions (*El* values labeled) through a straight 50 μm-wide and 25 μm-high rectangular microchannel under a constant flow rate of 250 μL/h: the left and right halves of each panel show the cropped superimposed image and particle PDF plot at the outlet expansion, respectively. The two dashed-line arrows on the image of PVP solution highlight the equilibrium positions of 5 μm particles near the corner of the channel. The scale bar represents 100 μm.

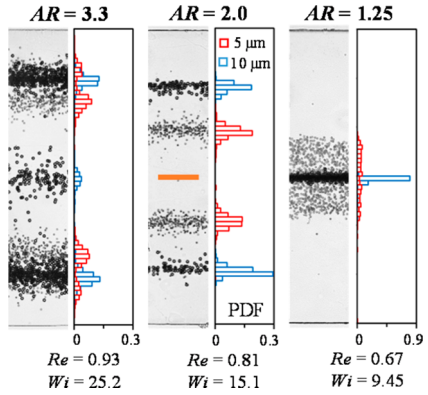

Figure 7. Effects of channel aspect ratio, AR, on the viscoelastic separation of 5 and 10 μm particles through straight 50 μm-wide rectangular microchannels at a fixed flow rate of 250 μL/h: the left and right halves of each panel show the cropped superimposed image and particle PDF plot at the outlet expansion, respectively. The scale bar represents 100 μm.

used polymer solutions through a 25 μm-deep microchannel at a fixed flow rate of 250 μL/h. In 8 wt % PVP solution, no separation takes place because both types of particles are focused into a single band around the centerline. This is attributed to the negligible shear thinning effects of this solution,[60] which produces a much weaker $F_{eL\rightarrow w}$ than $F_{eL\rightarrow c}$. However, a small number of 5 μm particles are observed to stay near the corners of the microchannel. This "secondary" equilibrium position, which was noticed in our earlier studies to disappear at higher flow rates,[44,47,55] however, remains in the whole range of flow rates (up to 500 μL/h, more images are shown in Figure S-2 of the Supporting Information) in our tests. It may be because the corner-directed F_{eL} is too strong in the PVP solution with a very large value of *El* = 368. The absence of 10 μm particles near the channel corner is surprising if we consider the fact that F_{eL} increases with particle size and F_{iL} is negligible at *Re* = 0.014. In the 50 ppm PAA solution, no separation is observed either because both types of particles are still dispersed with very weak focusing effects. This phenomenon is believed to be correlated with the cross-stream secondary flow in the PAA solution.[45,61,62]

Effects of Channel Aspect Ratio, AR. Figure 7 shows the channel aspect ratio, AR, effect on the viscoelastic separation of 5 and 10 μm particles in 1000 ppm PEO solution at a constant flow rate of 250 μL/h (see images for the other flow rates in Figure S-3 of the Supporting Information). The width of the rectangular microchannels is fixed at 50 μm while the height is varied from 15 to 25 μm and 40 μm, leading to a drop in both *Re* and *Wi*. In the 15 μm deep microchannel with AR = 3.3, three focusing positions are available for 10 μm particles, where one is along the channel centerline and the other two are each slightly within 1/3 of the channel half-width from the walls. The number of focusing positions is reduced to two off the centerline in the 25 μm deep channel (AR = 2.0) and to one along the centerline in the 40 μm deep channel (AR = 1.25). As *Re* and *Wi* both decrease in a deeper microchannel, the observed change in viscoelastic focusing positions of 10 μm particles is thought to be related to the increased shear gradients in the channel width direction, which enhances $F_{eL\rightarrow c}$ more than $F_{eL\rightarrow w}$. This hypothesis also explains why the focusing positions of 5 μm particles move inward from two off-center at AR = 3.3 and 2.0 to one along the centerline at AR = 1.25. The observation of single center-focusing position for both types of particles in a nearly square microchannel is consistent with earlier studies.[44,51,52]

Ternary Particle Separation. Figure 8 demonstrates a ternary separation of 3 μm, 5 and 10 μm particles in 1000 ppm

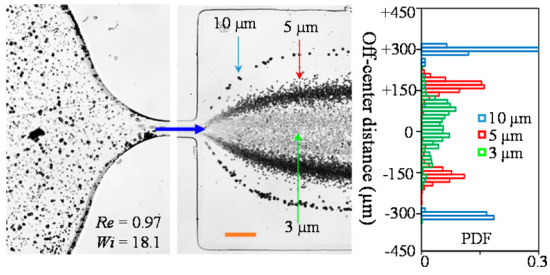

Figure 8. Viscoelastic separation of 3 μm-, 5 μm-, and 10 μm-diameter spherical particles in 1000 ppm PEO solution through a straight 50 μm-wide and 25 μm-high rectangular microchannel at a flow rate of 300 μL/h: (left) snapshot image at the channel inlet , (middle) superimposed images at the outlet expansion, and (right) particle PDF at the outlet expansion. The block arrow indicates the flow direction. The scale bar represents 100 μm.

PEO solution through a 25 μm deep microchannel at a flow rate of 300 μL/h (see images at other flow rates in Figure S-4 of the Supporting Information). Consistent with the binary separation in Figure 3, both 5 and 10 μm particles have two off-center focusing positions that still remain at about 1/3 of the channel half-width away from the channel centerline and walls, respectively. As $F_{eL\rightarrow c}$ is a weaker function of particle size than $F_{eL\rightarrow w}$, the smallest 3 μm particles in the mixture are mostly focused into a band around the centerline that has a slight overlapping with the 5 μm particle streams at its edges.

We divided each channel half-width into three zones: inner zone within 120 μm from the centerline, intermediate zone within 120 to 230 μm from the centerline, and outer zone beyond 230 μm from the centerline. The separation efficiency and purity, as defined below,

DOI: 10.1021/acs.analchem.6b03501
Anal. Chem. 2016, 88, 12303−12309

$$\text{efficiency} = \frac{\text{number of targeted particles inside a specific zone}}{\text{total number of targeted particles}} \quad (7)$$

$$\text{purity} = \frac{\text{number of targeted particles inside a specific zone}}{\text{total number of particles inside the same specific zone}} \quad (8)$$

for each type of particles in their respective preferred zones were calculated based on the experimental data of particle PDF in Figure 8 and are presented in Table 2. Specifically, the separation efficiency of 10 μm particles, as an example, was determined as the ratio of its number within the outer zone to its total number in all three zones, and the separation purity of 10 μm particles was determined as the ratio of its number within the outer zone to the total number of all three types of particles inside the same zone. The efficiency and purity of each particle type are 90% or better except for the purity of 3 μm particles. This is because the number of 5 μm particles (over 1550 counted) overwhelms the total of 3 μm (over 550 counted) and 10 μm (over 100 counted) particles in the video we analyzed. As a consequence, even a small percentage of 5 μm particles retained in the inner zone can significantly bring down the purity of 3 μm particles therein.

Table 2. Efficiency and Purity of the Ternary Particle Separation Shown in Figure 8

particles	number counts	preferred zone	efficiency (%)	purity (%)
10 μm	104	outer	96.2	95.2
5 μm	1576	intermediate	92.2	95.5
3 μm	570	inner	90.4	82.5

Summary of Parametric Effects on the Elastic Lift. On the basis of the above experimental results for the parametric effects on viscoelastic particle separation, we summarize in Table 3 the dependences of the two proposed components of elastic lift, $F_{eL\rightarrow w}$ and $F_{eL\rightarrow c}$, on multiple parameters in straight rectangular microchannels. Such a decomposition of the elastic lift into two components is analogous to that of the inertial lift into the wall- and shear gradient-induced components.[67,68] We note that the latter has been extensively used in the literature[16−19] to explain the inertial particle focusing behaviors though the specific scaling equations of the inertial lift components are currently still lacking.

Table 3. Parametric Dependences of the Elastic Lift in Viscoelastic Fluid Flows through Straight Rectangular Microchannels[a]

parameters	$F_{eL\rightarrow w}$	$F_{eL\rightarrow c}$	shift toward
particle size	stronger		wall
flow rate	stronger		wall
fluid elasticity		stronger	center
channel depth		stronger	center

[a]The last column shows the experimentally observed shifting of particle focusing positions with the increase of the corresponding experimental parameters under a negligible to weak inertia.

CONCLUSIONS

We have demonstrated continuous-flow sheath-free separations of both a binary 5 μm/10 μm and a ternary 3 μm/5 μm/10 μm particle mixture in 1000 ppm PEO solution through a simple straight rectangular microchannel. These separations arise from the flow-induced viscoelastic focusing effect that directs particles toward size-sensitive equilibrium positions. We have also conducted a comprehensive experimental study of the effects of flow rate, solvent viscosity, polymer concentration, polymer type, and channel aspect ratio on the binary particle separation in terms of four dimensionless numbers. To explain the observed shifting of particle focusing positions in this parametric study, we have proposed to break down the elastic lift into a center-directed component due to the fluid elasticity effects and a wall-directed component due to the fluid elasticity and shear thinning effects. These two components of elastic lift scale differently with the experimental parameters, which work either alone at relatively low flow rates or along with the inertial lift at increasing flow rates to produce the viscoelastic particle focusing in straight rectangular microchannels.

ASSOCIATED CONTENT

Supporting Information

The Supporting Information is available free of charge on the ACS Publications website at DOI: 10.1021/acs.analchem.6b03501.

Details on how to determine the rheology properties of the prepared polymer solutions that are presented in Table 1, the analysis of particle focusing in polymer solutions, the calculated values of dimensionless numbers in polymer solutions at different flow rates, and the experimental images for the parametric effects on the binary and ternary particle separations (PDF)

AUTHOR INFORMATION

Corresponding Author

*E-mail: xcxuan@clemson.edu. Phone: 864-656-5630. Fax: 864-656-7299.

ORCID

Xiangchun Xuan: 0000-0003-0158-4186

Notes

The authors declare no competing financial interest.

ACKNOWLEDGMENTS

This work was supported in part by NSF under Grant CBET-1150670.

REFERENCES

(1) Pamme, N. *Lab Chip* **2007**, *7*, 1644−1659.
(2) Gossett, D. R.; Weaver, W. M.; Mach, A. J.; Hur, S. C.; Tse, H. T.; Lee, W.; Amini, H.; Di Carlo, D. *Anal. Bioanal. Chem.* **2010**, *397*, 3249−3267.
(3) Karimi, A.; Yazdi, S.; Ardekani, A. M. *Biomicrofluidics* **2013**, *7*, 021501.
(4) Sajeesh, P.; Sen, A. K. *Microfluid. Nanofluid.* **2014**, *17*, 1−52.
(5) Shields, C. W., IV; Reyes, C. D.; Lopez, G. P. *Lab Chip* **2015**, *15*, 1230−1249.
(6) Laurell, T.; Petersson, F.; Nilsson, A. *Chem. Soc. Rev.* **2007**, *36*, 492−506.
(7) Wang, Z.; Zhe, J. *Lab Chip* **2011**, *11*, 1280−1285.
(8) Pethig, R. *Biomicrofluidics* **2010**, *4*, 022811.

DOI: 10.1021/acs.analchem.6b03501
Anal. Chem. 2016, 88, 12303−12309

(9) Regtmeier, J.; Eichhorn, R.; Viefhues, M.; Bogunovic, L.; Anselmetti, D. *Electrophoresis* **2011**, *32*, 2253−2273.
(10) Tsutsui, H.; Ho, C. M. *Mech. Res. Commun.* **2009**, *36*, 92−103.
(11) McGrath, J.; Jimenez, M.; Bridle, H. *Lab Chip* **2014**, *14*, 4139−4158.
(12) Hejazian, M.; Li, W.; Nguyen, N. T. *Lab Chip* **2015**, *15*, 959−970.
(13) Zhao, W.; Cheng, R.; Miller, J.; Mao, L. *Adv. Funct. Mater.* **2016**, *26*, 3916−3932.
(14) Kim, S. B.; Yoon, S. Y.; Sung, H. J.; Kim, S. S. *Anal. Chem.* **2008**, *80*, 2628−2630.
(15) Kayani, A. A.; Khoshmanesh, K.; Ward, S. A.; Mitchell, A.; Kalantar-zadeh, K. *Biomicrofluidics* **2012**, *6*, 031501.
(16) Di Carlo, D. *Lab Chip* **2009**, *9*, 3038−3046.
(17) Martel, J. M.; Toner, M. *Annu. Rev. Biomed. Eng.* **2014**, *16*, 371−396.
(18) Amini, H.; Lee, W.; Di Carlo, D. *Lab Chip* **2014**, *14*, 2739−2761.
(19) Zhang, J.; Yan, S.; Yuan, D.; Alici, G.; Nguyen, N. T.; Warkiani, M. E.; Li, W. *Lab Chip* **2016**, *16*, 10−34.
(20) Kim, J. Y.; Ahn, S. W.; Lee, S. S.; Kim, J. M. *Lab Chip* **2012**, *12*, 2807−2814.
(21) De Santo, I.; D'Avino, G.; Romeo, G.; Greco, F.; Netti, P. A.; Maffettone, P. L. *Phys. Rev. Appl.* **2014**, *2*, 064001.
(22) Lim, E. J.; Ober, T.; Edd, J. F.; Desai, S. P.; Neal, D.; Bong, K. W.; Doyle, P. S.; McKinley, G. H.; Toner, M. *Nat. Commun.* **2014**, *5*, No. 4120, DOI: 10.1038/ncomms5120.
(23) Trofa, M.; Vocciante, M.; D'Avino, G.; Hulsen, M. A.; Greco, F.; Maffettone, P. L. *Comput. Fluids* **2015**, *107*, 214−223.
(24) D'Avino, G.; Maffettone, P. L. *J. Non-Newtonian Fluid Mech.* **2015**, *215*, 80−104.
(25) Kim, B.; Kim, J. M. *Biomicrofluidics* **2016**, *10*, 024111.
(26) D'Avino, G.; Romeo, G.; Villone, M. M.; Greco, F.; Netti, P. A.; Maffettone, P. L. *Lab Chip* **2012**, *12*, 1638−1645.
(27) Romeo, G.; D'Avino, G.; Greco, F.; Netti, P. A.; Maffettone, P. L. *Lab Chip* **2013**, *13*, 2802−2807.
(28) Seo, K. W.; Byeon, H. J.; Huh, H. K.; Lee, S. J. *RSC Adv.* **2014**, *4*, 3512−3520.
(29) Leshansky, A. M.; Bransky, A.; Korin, N.; Dinnar, U. *Phys. Rev. Lett.* **2007**, *98*, 234501.
(30) Del Giudice, F.; Romeo, G.; D'Avino, G.; Greco, F.; Netti, P. A.; Maffettone, P. L. *Lab Chip* **2013**, *13*, 4263−4271.
(31) Seo, K. W.; Kang, Y. J.; Lee, S. J. *Phys. Fluids* **2014**, *26*, 063301.
(32) Del Giudice, F.; D'Avino, G.; Greco, F.; Netti, P. A.; Maffettone, P. L. *Microfluid. Nanofluid.* **2015**, *19*, 95−104.
(33) Lee, D. L.; Brenner, H.; Youn, J. R.; Song, Y. S. *Sci. Rep.* **2013**, *3*, No. 3258, DOI: 10.1038/srep03258.
(34) Cha, S.; Kang, K.; You, J. B.; Im, S. G.; Kim, Y.; Kim, J. M. *Rheol. Acta* **2014**, *53*, 927−933.
(35) Yuan, D.; Zhang, J.; Yan, S.; Pan, C.; Alici, G.; Nguyen, N. T.; Li, W. H. *Biomicrofluidics* **2015**, *9*, 044108.
(36) Xiang, N.; Zhang, X.; Dai, Q.; Cheng, J.; Chen, K.; Ni, Z. *Lab Chip* **2016**, *16*, 2626−2635.
(37) Cha, S.; Shin, T.; Lee, S. S.; Shim, W.; Lee, G.; Lee, S. J.; Kim, Y.; Kim, J. M. *Anal. Chem.* **2012**, *84*, 10471−10477.
(38) Seo, K. W.; Ha, Y. R.; Lee, S. J. *Appl. Phys. Lett.* **2014**, *104*, 213702.
(39) Bae, Y. B.; Jang, H. K.; Shin, T. H.; Phukan, G.; Tran, T. T.; Lee, G.; Hwang, W. R.; Kim, J. M. *Lab Chip* **2016**, *16*, 96−103.
(40) Ha, B.; Park, J.; Destgeer, G.; Jung, J. J.; Sung, H. J. *Anal. Chem.* **2016**, *88*, 4205−4210.
(41) Yuan, D.; Zhang, J.; Yan, S.; Peng, G.; Zhao, Q.; Alici, G.; Du, H.; Li, W. H. *Electrophoresis* **2016**, *37*, 2147−2155.
(42) Wu, Z.; Hjort, K.; Wicher, G.; Svenningsen, A. F. *Biomed. Microdevices* **2008**, *10*, 631−638.
(43) Nam, J.; Lim, H.; Kim, D.; Jung, H.; Shin, S. *Lab Chip* **2012**, *12*, 1347−1354.
(44) Lu, X.; Xuan, X. *Anal. Chem.* **2015**, *87*, 6389−6396.
(45) Lim, H.; Nam, J.; Shin, S. *Microfluid. Nanofluid.* **2014**, *17*, 683−692.
(46) Kang, K.; Lee, S. S.; Hyun, K.; Lee, S. J.; Kim, J. M. *Nat. Commun.* **2013**, *4*, No. 2567, DOI: 10.1038/ncomms3567.
(47) Lu, X.; Xuan, X. *Anal. Chem.* **2015**, *87*, 11523−11530.
(48) Nam, J.; Namgung, B.; Lim, C. T.; Bae, J. E.; Leo, H. L.; Cho, K. S.; Kim, S. *J. Chromatogr. A* **2015**, *1406*, 244−250.
(49) Nam, J.; Tan, J. K.; Khoo, B. L.; Namgung, B.; Leo, H. L.; Lim, C. T.; Kim, S. *Biomicrofluidics* **2015**, *9*, 064117.
(50) Nam, J.; Shin, Y.; Tan, J. K. S.; Lim, Y. B.; Lim, C. T.; Kim, S. *Lab Chip* **2016**, *16*, 2086−2092.
(51) Yang, S. Y.; Kim, J. Y.; Lee, S. J.; Lee, S. S.; Kim, J. M. *Lab Chip* **2011**, *11*, 266−273.
(52) Ahn, S. W.; Lee, S. S.; Lee, S. J.; Kim, J. M. *Chem. Eng. Sci.* **2015**, *126*, 237−243.
(53) Yang, S.; Lee, S. S.; Ahn, S. W.; Kang, K.; Shim, W.; Lee, G.; Hyun, K.; Kim, J. M. *Soft Matter* **2012**, *8*, 5011−5019.
(54) Liu, C.; Xue, C.; Chen, X.; Shan, L.; Tian, Y.; Hu, G. *Anal. Chem.* **2015**, *87*, 6041−6048.
(55) Lu, X.; Zhu, L.; Hua, R.; Xuan, X. *Appl. Phys. Lett.* **2015**, *107*, 264102.
(56) Li, D.; Lu, X.; Song, Y.; Wang, J.; Li, D.; Xuan, X. *Biomicrofluidics* **2016**, *10*, 054104.
(57) Ho, B. P.; Leal, L. G. *J. Fluid Mech.* **1976**, *76*, 783−799.
(58) Huang, P. Y.; Feng, J.; Hu, H. H.; Joseph, D. D. *J. Fluid Mech.* **1997**, *343*, 73−94.
(59) Li, G.; McKinley, G. H.; Ardekani, A. M. *J. Fluid Mech.* **2015**, *785*, 486−505.
(60) Bird, R. B.; Armstrong, R.; Hassager, O. *Dynamics of Polymeric Liquids*; Wiley Interscience Publication: New York, 1987.
(61) Gervang, B.; Larsen, P. S. *J. Non-Newtonian Fluid Mech.* **1991**, *39*, 217−237.
(62) Villone, M. M.; D'Avino, G.; Hulsen, M. A.; Greco, F.; Maffettone, P. L. *J. Non-Newtonian Fluid Mech.* **2013**, *195*, 1−8.
(63) Di Carlo, D.; Irimia, D.; Tompkins, R. G.; Toner, M. *Proc. Natl. Acad. Sci. U. S. A.* **2007**, *104*, 18892−18897.
(64) Huang, P. Y.; Joseph, D. D. *J. Non-Newtonian Fluid Mech.* **2000**, *90*, 159−185.
(65) Romeo, G.; D'Avino, G.; Greco, F.; Netti, P. A.; Maffettone, P. L. *Lab Chip* **2013**, *13*, 2802−2807.
(66) Lu, X.; Xuan, X. *Anal. Chem.* **2015**, *87*, 4560−4565.
(67) Ho, B. P.; Leal, L. G. *J. Fluid Mech.* **1974**, *65*, 365−400.
(68) Vasseur, P.; Cox, R. G. *J. Fluid Mech.* **1976**, *78*, 385−413.

DOI: 10.1021/acs.analchem.6b03501
Anal. Chem. 2016, 88, 12303−12309